SCIENCE CHINA
Life Sciences

•COVER ARTICLE•

January 2020 Vol.63 No.1: 1–17
https://doi.org/10.1007/s11427-019-9817-6

Temporal regulation of prenatal embryonic development by paternal imprinted loci

Qing Li[1†], Yuanyuan Li[1†], Qi Yin[1†], Shuo Huang[2†], Kai Wang[1†], Liangchai Zhuo[2], Wei Li[1], Boran Chang[1] & Jinsong Li[1,2*]

[1]*State Key Laboratory of Cell Biology, CAS Center for Excellence in Molecular Cell Science, Shanghai Key Laboratory of Molecular Andrology, Shanghai Institute of Biochemistry and Cell Biology, Chinese Academy of Sciences, University of Chinese Academy of Sciences, Shanghai 200031, China;*

[2]*School of Life Science and Technology, Shanghai Tech University, Shanghai 201210, China*

Received July 10, 2019; accepted August 9, 2019; published online September 17, 2019

Paternal imprinted genes (*H19* and *Gtl2*) are pivotal for prenatal embryonic development in mice. Nongrowing oocytes and sperm- or oocyte-originated haploid embryonic stem cells (haESCs) carrying both *H19*-DMR (differentially DNA-methylated region) and *IG* (intergenic)-DMR deletions that partially mimic paternal imprinting of *H19-Igf2* and *Dlk1-Dio3* can be employed as sperm replacement to efficiently support full-term embryonic development. However, how *H19*-DMR and *IG*-DMR act together to regulate embryonic development is still largely unknown. Here, using androgenetic haESC (AG-haESC)-mediated semi-cloned (SC) technology, we showed that paternal *H19*-DMR and *IG*-DMR are not essential for pre-implantation development of SC embryos generated through injection of AG-haESCs into oocytes. *H19*-DMR plays critical roles before 12.5 days of gestation while *IG*-DMR is essential for late-gestation of SC embryos. Interestingly, we found that combined deletions of *H19* and *H19*-DMR can further improve the efficiency of normal development of SC embryos at mid-gestation compared to DKO SC embryos. Transcriptome and histology analyses revealed that *H19* and *H19*-DMR combined deletions rescue the placental defects. Furthermore, we showed that *H19*, *H19*-DMR and *IG*-DMR deletions (TKO) give rise to better prenatal and postnatal embryonic development of SC embryos compared to DKO. Together, our results indicate the temporal regulation of paternal imprinted loci during embryonic development.

imprinted loci, semi-cloned technology, temporal regulation, *H19-Igf2*, *Dlk1-Dio3*, embryonic development

Citation: Li, Q., Li, Y., Yin, Q., Huang, S., Wang, K., Zhuo, L., Li, W., Chang, B., and Li, J. (2020). Temporal regulation of prenatal embryonic development by paternal imprinted loci. Sci China Life Sci 63, 1–17. https://doi.org/10.1007/s11427-019-9817-6

INTRODUCTION

In the 1970s, mouse parthenogenetic (PG) embryos were generated through chemical activation of mature oocytes; however, the PG embryos could not survive after 10 days of gestation (Graham, 1970; Kaufman, 1973; Tarkowski, 1975). In 1984, two elegant embryological experiments achieved by construction of mouse embryos carrying only paternal or maternal genome provided direct evidence to demonstrate nonequivalence of parental genome, the concept of genomic imprinting (McGrath and Solter, 1984; Surani et al., 1984). Genomic imprinting, an epigenetic mechanism that results in parent-of-origin specific gene expression, plays essential roles in the regulation of mammalian embryonic and extra-embryonic development (Barlow and Bartolomei, 2014; Ferguson-Smith, 2011).

Among the 151 reported murine imprinted genes (http://www.mousebook.org/imprinting-gene-list), the *H19-Igf2* locus, the first identified imprinted region, is critical for

†Contributed equally to this work
*Corresponding author (email: jsli@sibcb.ac.cn)

normal prenatal growth and placentation and is regulated by differential DNA methylation (*H19*-DMR) (Arney, 2003; Bartolomei et al., 1991; Cleaton et al., 2014; DeChiara et al., 1991). *H19*-DMR, located 2–4 kb upstream from the start of the transcription start site (Thorvaldsen et al., 1998; Tremblay et al., 1997), is essential for establishing the pattern of imprinting by which *H19*, a non-coding RNA, is exclusively expressed from the maternal chromosome (Bartolomei et al., 1991) and only the paternal *Igf2* is active (DeChiara et al., 1991). On the maternal chromosome, the DMR is hypomethylated and bound by the zinc-finger protein CCCTC-binding factor (CTCF) (Bell et al., 1999), leading to the establishment of an insulator that acts as a barrier to influence the neighboring *cis*-acting elements and silence *Igf2* on the maternal allele (Bell and Felsenfeld, 2000; Hark et al., 2000). On the paternal chromosome, the DMR is hypermethylated and not bound by CTCF, thus allowing downstream enhancers to activate the paternal *Igf2* gene (Bell and Felsenfeld, 2000; Hark et al., 2000). *H19* knockout mice are viable and fertile, but present an overgrowth phenotype (Leighton et al., 1995). In contrast, overexpression of *H19* was deleterious to embryo development after embryonic day 14 (E14) (Brunkow and Tilghman, 1991). Deletion of *Igf2* leads to fetal and placental growth restriction (Constância et al., 2002; DeChiara et al., 1990), whereas overexpression of the *Igf2* by imprint relaxation (biparental expression) leads to placental and fetal overgrowth (Eggenschwiler et al., 1997). Interestingly, paternal deletion of *H19*-DMR, although with *H19* activation and decreased *Igf2* expression, results in overall normal growth in the mouse (Leighton et al., 1995; Thorvaldsen et al., 1998). Taken together, the *H19-Igf2* locus influences embryonic development probably by regulating the expression of *Igf2*, which plays important roles in embryonic and placental development (Burns and Hassan, 2001; Morrione et al., 1997; Sibley et al., 2004).

The *Dlk1-Dio3* locus is another essential imprinted region for embryonic development, in which, *Gtl2* and *Dlk1* are reciprocally expressed. *Gtl2* is expressed from the maternal allele, while *Dlk1* is expressed exclusively from the paternal allele (Schmidt et al., 2000; Takada et al., 2000) and controlled by intergenic germline-derived (*IG*)-DMR (Lin et al., 2003; Takada et al., 2002). Deletion of *IG*-DMR from the maternal chromosome leads to loss of imprinting (LOI) in this locus and causes embryonic lethal after E16, but paternal deletion does not change the imprinting state of the region, leading to normal embryonic development in the resultant mouse (Lin et al., 2003).

With the identification of the imprinted genes, efforts have been made to remove the paternal imprinting barriers that prevent the normal development of mouse bi-maternal embryos. Interestingly, PG embryos, which contained one set of chromosomes from an imprinting-free neonate-derived non-growing (ng) oocyte and the other from a fully grown (fg) oocyte, successfully developed to a normal-sized fetus with a well-developed placenta on day 13.5 of gestation, 3 days longer than previously reported for parthenogenetic development (Kono et al., 1996). Furthermore, using the same system, in ng oocytes harboring a 3-kilobase (kb) deletion covering the *H19* transcription unit, the reconstructed parthenotes could develop to day 17.5 of gestation (Kono et al., 2002). Moreover, in ng oocytes carrying a 13-kb deletion including both *H19* and *H19*-DMR, a small proportion of the parthenotes could develop to term and grow to adulthood (Kono et al., 2004). Surprisingly, the birth rate of the reconstructed bi-maternal embryos was greatly improved when both *H19*-DMR and *IG*-DMR were deleted in the ng oocytes (Kawahara et al., 2007), indicating that *H19-Igf2* and *Dlk1-Dio3* imprinted clusters are the main paternal imprinting barriers to normal development of bi-maternal fetus.

Recently, we and others generated mouse androgenetic haploid embryonic stem cells (AG-haESCs) that can be used as “artificial spermatids” to generate live semi-cloned (SC) mice through intracytoplasmic injection (ICAHCI) into mature oocytes (Li et al., 2012; Yang et al., 2012). We further optimized the SC technology through the generation of AG-haESCs carrying both *H19*-DMR and *IG*-DMR deletions (DKO-AG-haESCs) that can efficiently support the development of SC embryos (Zhong et al., 2015). Interestingly, oocyte-originated haploid ESCs, with both *H19*-DMR and *IG*-DMR removed, could also be used as sperm replacement to produce bi-maternal mice efficiently (Li et al., 2016; Zhong et al., 2016). Importantly, AG-haESCs mediated SC technology combined with CRISPR-Cas9 opens new avenues for genetic analyses *in vivo* (Jiang et al., 2019; Li et al., 2018; Wang and Li, 2019; Wei et al., 2017; Zhong et al., 2015). However, it is still not clear how *H19*-DMR and *IG*-DMR coordinately regulate SC embryonic development.

In this study, we sought to determine the roles of *H19*-DMR and *IG*-DMR in SC embryonic development. Our results showed that the *H19*-DMR and *IG*-DMR are dispensable for the pre-implantation development of SC embryos. Furthermore, we showed that *H19*-DMR is essential for the development of SC embryos before mid-gestation and *IG*-DMR is critical for late-gestation. In addition, the newly established AG-haESCs carrying triple deletions (TKO), including *H19*, *H19*-DMR and *IG*-DMR, can further improve the efficiency of producing viable, normal-sized, and fertile SC mice through ICAHCI.

RESULTS

Paternal *H19*-DMR and *IG*-DMR are not essential for the pre-implantation development of SC embryos

In our previous work, we have shown that double deletions

of *H19*-DMR and *IG*-DMR (DKO) in mouse AG-haESCs significantly improve the birth rate of SC mice (Zhong et al., 2015). Interestingly, we found that DKO does not change the transcriptional and methylation profiles in haploid ESCs, suggesting that both deletions may not function in cells and probably play roles in SC embryonic development upon injection of DKO cells into oocytes. Therefore, in this study, we sought to define how *H19*-DMR and *IG*-DMR regulate development of SC embryos. To this end, we chose wild-type (WT) AG-haESCs (AGH-OG3) and DKO-AG-haESCs ($H19^{\triangle DMR}$-$IG^{\triangle DMR}$-AGH-OG3) carrying an *Oct4-eGFP* transgene, which were derived in our previous studies (Yang et al., 2012; Zhong et al., 2015). EGFP fluorescence activation and PCR analyses confirmed that cells carried the expected transgene and deletions (Figure S1A and B in Supporting Information). Haploidy of AG-haESCs was stably maintained by fluorescence-activated cell sorting (FACS)-based enrichment of haploid cells every 4–6 passages (Figure S1C in Supporting Information). We first checked the expression of the imprinted genes regulated by *H19*-DMR and *IG*-DMR through quantitative reverse transcription PCR (RT-qPCR) analysis and found, as expected, *H19* and *Gtl2* were down-regulated in DKO haploid cells, while *Igf2* and *Dio3* were up-regulated (Figure S1D in Supporting Information). We then analyzed the transcriptomes of both cells and found that, consistent with previous results (Zhong et al., 2015), WT and DKO haploid cells exhibited a high correlation based on all genes (R=0.99) (Figure S1E in Supporting Information) and all known imprinted genes (R=0.99) (Figure S1F in Supporting Information). Interestingly, *Fthl17*, the X-linked maternal imprinted gene that may contribute to the early sex differentiation before gonadal differentiation (Kobayashi et al., 2010), was also downregulated in DKO cells (Figure S1D and F in Supporting Information). Together, removal of *H19*-DMR and *IG*-DMR in AG-haESCs could mimic the methylation state of *H19*-DMR and *IG*-DMR in sperm that is lost during haploid ESC derivation and passaging in 2i medium (Choi et al., 2017; Yagi et al., 2017; Yang et al., 2012) (Figure S1G in Supporting Information), leading to DKO haploid ESCs with decreased expression of *H19* and *Gtl2*, two critical paternal imprinted genes for embryonic development.

We next investigated whether *H19*-DMR and *IG*-DMR deletions are beneficial to pre-implantation development of SC embryos generated by injection of WT or DKO AG-haESCs into mature oocytes (ICAHCI). The results showed that the efficiency of well-shaped blastocysts was similar among sperm carrying a *Oct4-eGFP* transgene (control), WT and DKO AG-haESCs (Figure 1A and B). To further characterize the blastocysts produced from different haploid cells, we separated inner cell mass (ICM) and trophectoderm (TE) and carried out low-cell-number (around 10 cells) RNA-seq analysis (Figure S2A–C in Supporting Information). Hierarchical clustering and principal component analysis (PCA) of transcriptome data showed that all ICM samples were clustered together, but separated from TE samples which were also exclusively clustered together, indicating that the transcriptome differences between all samples are mainly caused by their different lineage origins (Figure 1C, Figure S2D in Supporting Information). Pearson correlation analysis further confirmed the similarity among different blastocysts (Figure 1D) and all imprinted genes exhibited similar expression patterns (Figure 1E). Moreover, the expression levels of *H19*, *Igf2*, *Gtl2* and *Dlk1* were low in all tested ICM and TE samples (Figure 1E and F), suggesting that *H19-Igf2* and *Dlk1-Dio3* imprinted clusters may not function in pre-implantation development of SC embryos. Therefore, we examined the expression of *H19*, *Igf2*, *Gtl2* and *Dlk1* in control and SC embryos after implantation and found gradually increased expression of all four genes following embryonic development from E3.5 to E9.5 (Figure 1G), implying that DKO could rescue transcriptional defects of *H19* and *Igf2* in SC embryos from WT haploid cells. These data suggest that paternal *H19*-DMR and *IG*-DMR are not essential for pre-implantation development of SC embryos.

H19-DMR and *IG*-DMR deletions (DKO) significantly improve the developmental potential of SC embryos during mid-gestation

We next examined the effect of DKO on prenatal development by transplantation of 2-cell SC embryos produced through ICAHCI of WT or DKO haploid cells into oviducts of pseudo-pregnant females (Figure 2A). A total of 2,173 WT and 1,352 DKO SC two-cell embryos were transplanted. Dissection of SC embryos in pregnant females day-by-day from E6.5 to E12.5 revealed that DKO SC embryos implanted at significantly higher efficiency compared with WT SC embryos (41.9% vs. 34.6%) (Figure 2B). Furthermore, the developmental potential of DKO SC was significantly higher than WT SC embryos at E12.5 (Figure 2C). Moreover, higher frequency of abnormal embryos (degeneration or morphological abnormalities) was displayed in the WT group starting from E8.5 (Figure 2D and E). Interestingly, we found that most abnormal DKO SC embryos degenerated by E10.5 and thereafter DKO embryos exhibited similar developmental potential at different stages until birth, whereas a high ratio of WT SC embryos showed both developmental retardation and degeneration and continued to display developmental failure at the following stages (Figure 2E–G), suggesting that DKO rescues the developmental defects of SC embryos before mid-gestation.

We next carefully compared the morphological differences between DKO and WT SC embryos. We observed that a high ratio of WT SC fetuses was alive with normal heartbeat on

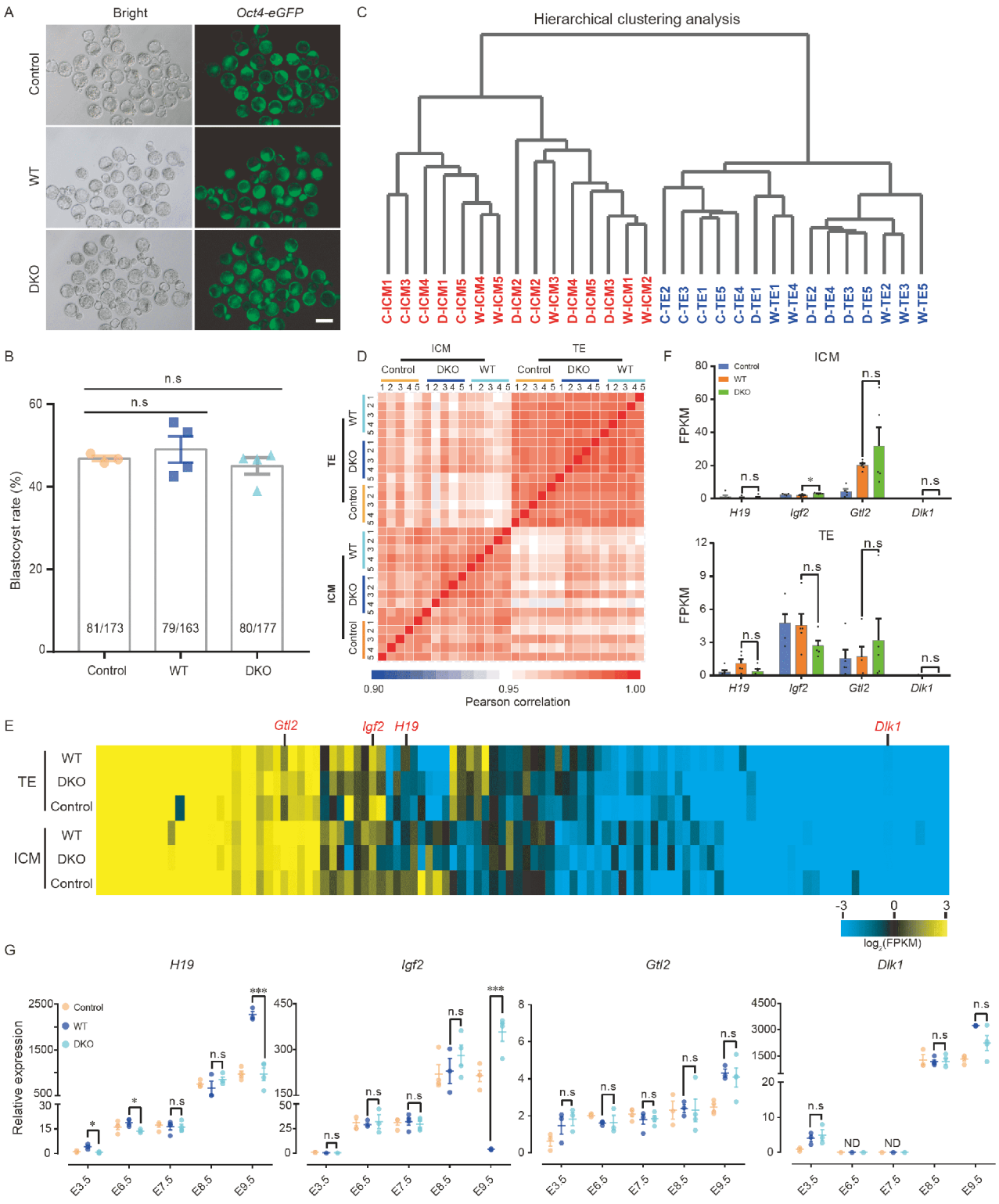

Figure 1 Paternal *H19*-DMR and *IG*-DMR are dispensable for the pre-implantation development of SC embryos. A and B, Representative images of blastocysts (A) and the efficiency of blastocysts derived from sperm (control), WT and DKO-AG-haESCs (B), showing similar developmental potential among different haploid cells. Numbers in the bars show the number of blastocysts/two-cell embryos. Scale bar, 100 μm. C and D, Hierarchical clustering analysis (C) and correlation heatmap (D) of RNA-seq data from ICMs (5 replicates) and TEs (5 replicates) obtained from different haploid donors. C, control embryos derived from intracytoplasmic sperm injection (ICSI); W, embryos from intracytoplasmic WT-AG-haESC injection; D, embryos from DKO-AG-haESC. E, Heatmap showing expression patterns of imprinted genes in TE (top) and ICM (bottom). The gene expression levels were measured as $\log_2$ (FPKM). F, The expression levels of *H19*, *Igf2*, *Gtl2* and *Dlk1* in ICM and TE. G, Transcriptional analysis of *H19*, *Igf2*, *Gtl2* and *Dlk1* genes among control (ICSI), WT and DKO embryos from E3.5 to E9.5 (n=3 embryos). The expression values were normalized to that of *Gapdh*. All error bars in B, F and G indicate the average mean ±SEM. *, P<0.05; ***, P<0.001; n.s, no significant difference.

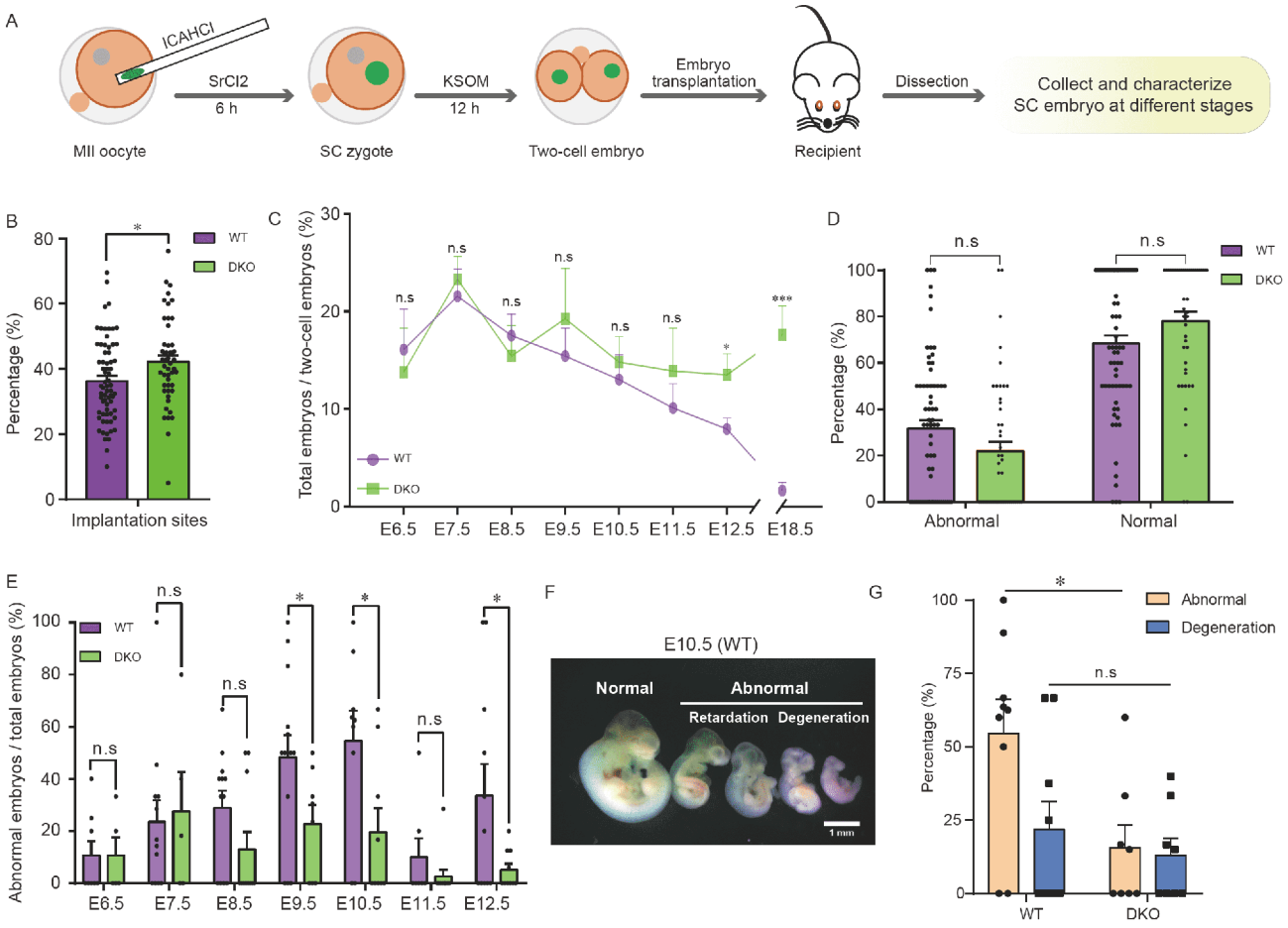

Figure 2 Analysis of developmental potential of SC embryos at different stages. A, Schematic diagram of developmental potential analysis of SC embryos generated via ICAHCI of WT or DKO AG-haESCs. B, Summary of the average implantation rate of WT (n=68 recipients) and DKO (n=49 recipients) SC embryos dissected from E6.5 to E12.5. C, Comparison of the developmental efficiency on different embryonic days between WT and DKO SC embryos. E, embryonic day. D, The ratios of abnormal and normal SC embryos (from E6.5 to E12.5) in transferred 2-cell embryos derived from WT (n=68 recipients) and DKO (n=49 recipients). E, Comparison of the ratios of abnormal SC embryos on different embryonic days (from E6.5 to E12.5) between WT and DKO groups. F, Representative images of E10.5 SC embryos produced from WT AG-haESCs. G, The ratios of abnormal and degeneration embryos are shown. Each dark spot in B, D, E and G represents the result of one recipient mouse. All error bars in B–E and G indicate the average mean ±SEM. *, P<0.05; ***, P<0.001; n.s, no significant difference.

E8.5 (Figure 2C), but most of them exhibited developmental arrest starting from day 10.5 of gestation (Figure 3A). In particular, both fetal and placental weights were significantly lower in WT SC conceptus than those of the DKO SC conceptus on E12.5 (Figure 3B). Interestingly, the blood vessels of amniotic sac and umbilical cord were thinner and shorter in the WT SC conceptus, which may influence nutrient and gas-exchange with the mother (Figure 3C). The mature placenta contains three main layers: the labyrinth, which constitutes the main nutrient and gas-exchange surface; the basal zone, which consists of spongiotrophoblast, glycogen cells and different giant cell subtypes; and the maternally-derived decidua (Rossant and Cross, 2001). Hematoxylin eosin (HE) staining of placentas indicated that the WT SC placentas had smaller total areas and increased ratio of decidual areas compared with those of the DKO (Figure 3D and E). In addition, we found that the glycogen cells in the basal zone were dramatically reduced in WT placentas (Figure 3D).

We next assessed the expression of critical imprinted genes in placentas via RT-qPCR. As expected, *H19* was over-expressed whereas *Igf2* expression was significantly decreased in WT placentas (Figure 3F), which may account for the reduced glycogen cells in WT SC placentas (Lopez et al., 1996). *Igf2* is an important regulator in maintenance of the balance between supply and demand systems that is crucial to fine-tune mammalian growth (Angiolini et al., 2011; Constância et al., 2005). We then tested the expression of glucose transporter genes (*Slc2a1* and *Slc2a3*) and amino acid transporter genes (*Slc38a1*, *Slc38a2*, and *Slc38a4*) in E12.5 placentas. The results showed that *Slc2a3* and *Slc38a2* were significantly increased in the WT SC placentas (Figure S3A in Supporting Information), probably leading to increased nutrient transfer that adapts the nutrient supply to

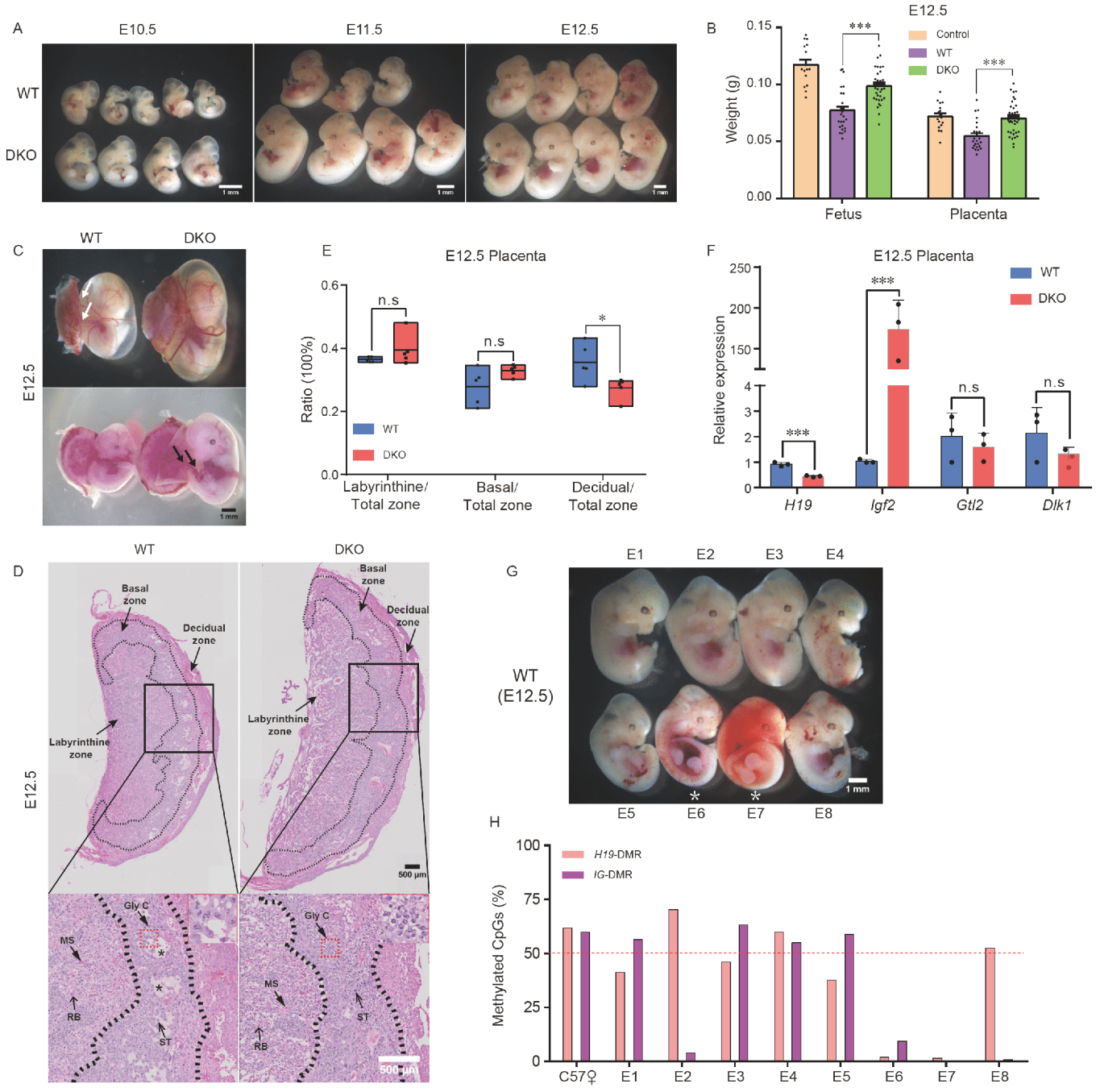

Figure 3 *H19*-DMR and *IG*-DMR double knock-out rescues the retardation of SC placentas at mid-gestation. A, Representative images of live SC embryos (E10.5 to E12.5) derived from WT (top panel) and DKO (bottom panel) AG-haESCs show retarded growth in WT group. B, The fetal and placental weights of E12.5 embryos derived from sperm (control, n=17), WT (n=25) and DKO (n=36) AG-haESCs, showing severe retardation in WT embryos and placentas compared with control and DKO embryos. C, E12.5 conceptus derived from WT and DKO AG-haESCs. An obvious gap (white arrow) between the placenta and visceral yolk sac shows in WT fetus (top panel). The well-developed umbilical cord (black arrows) shows in the DKO fetus (bottom panel). Experiments were repeated five times independently, with similar results. D, Whole mount images of SC placentas (E12.5) (top panel). Black boxes in the top panel are magnified in the bottom panel. The total placental area is smaller in the WT compared with that in DKO. Fewer glycogen cells (Gly C) exist in the basal zone of the placenta from the WT compared with DKO, shown in red dashed boxes. Asterisks show vacuolation in WT placentas. MS, maternal sinusoid; RB, red blood cells; ST, spongiotrophoblast. Experiments were repeated five times independently, with similar results. E, The ratios of labyrinthine zone, basal zone and decidual zone to total placental areas of WT and DKO placentas (E12.5), indicating increased decidual area in WT placentas. Five placentas for each group and at least 5 sections per placenta were analyzed. Middle lines are shown as the mean. F, Transcriptional analysis of *H19*, *Igf2*, *Gtl2* and *Dlk1* genes in WT and DKO placentas (3 placentas for each group). The expression values were normalized to that of *Gapdh*. Data are shown as the average mean±SEM in B and F. *, P<0.05; ***, P<0.001; n.s, no significant difference. G and H, Eight E12.5 SC embryos from WT cells (E1 to E8) (G) and their methylation state of the *H19*-DMR and *IG*-DMR (H). Embryos with a white asterisk are dead. The dotted line shows theoretical value of methylation, 50%. E denotes embryo in Figure G.

fetal demand (Constância et al., 2005). We also found that estrogen receptor (*Esr1* and *Esr2*) and androgen receptor (*Ar*) were highly expressed in the WT placentas, whereas the inactivator of testosterone and estrogen (hydroxysteroid 17-beta dehydrogenase 2, *Hsd17b2*) showed no difference (Figure S3A in Supporting Information), consistent with previous observations that excess maternal androgen reduces placental and fetal weights (Sun et al., 2012). Furthermore, WT SC fetuses died progressively from E11.5 to E15.5 (Figure S3B and C in Supporting Information) and only two from a total of 308 WT SC embryos (0.6%) derived from AGH-OG3 cells with late passages (over passage 40) survived on E18.5 (Figure S3D and E in Supporting Information). These results indicate that the developmental failure of WT SC embryos is mainly caused by placental defects, which can be rescued by *H19*-DMR and *IG*-DMR deletions.

IG-DMR deletion alone fails to rescue the developmental retardation of SC embryos before E12.5

Interestingly, we observed that the two dead embryos (E12.5) from WT AG-haESCs both lost DNA methylation at the *H19*-DMR locus (Figure 3G and H). In contrast, loss of DNA methylation at the *IG*-DMR locus appeared in both live and dead embryos on E12.5 (Figure 3G and H). These results suggest that *H19*-DMR methylation is essential for SC embryonic development before mid-gestation, while *IG*-DMR may not be important. To further explore their roles in SC embryonic development, we firstly deleted the 4 kb region of *IG*-DMR (Lin et al., 2003) in AGH-OG3 cells using CRISPR/Cas9 technology (Figure 4A). Two single guide RNAs (sgRNAs) targeting upstream and downstream of the region were designed and ligated to pX330-*mCherry* plasmid (Wu et al., 2013) and transfected into haploid cells, leading to two stable cell lines, termed $IG^{\triangle DMR}$-AGH-OG3-1 and 2 (Figure S4A in Supporting Information). Interestingly, these two cell lines were free of DNA methylation at *H19*-DMR (Figure S4B in Supporting Information). ICAHCI analysis indicated that *IG*-DMR deletion did not improve the developmental potential of SC embryos, and the percentage of abnormal SC embryos was comparable to that of WT SC embryos (Figure 4B). Meanwhile, the live E12.5 fetuses of $IG^{\triangle DMR}$ exhibited growth-retarded phenotypes in both embryos and placentas (Figure 4C and D). Further, placental defects were more severe than in WT fetuses (Figure 4D–F, Figure S4C in Supporting Information). DNA methylation at *H19*-DMR was absent in $IG^{\triangle DMR}$ SC embryos (Figure S4D and E in Supporting Information), resulting in misexpression of *H19* and *Igf2* in $IG^{\triangle DMR}$ SC placentas (Figure 4G). As expected, SC embryos with paternal *IG*-DMR deletion alone rarely developed to day 18.5 gestation (Figure 4H). These results indicate that *IG*-DMR deletion in AG-haESCs is dispensable for SC embryo development before mid-gestation.

$H19^{\Delta 13kb}$ rescues developmental defects of SC embryos at mid-gestation

Having shown that *IG*-DMR is not critical for SC embryonic development before mid-gestation, we next examined the role of *H19*-DMR in SC embryonic development. Since *H19*-DMR deletion cannot totally repress paternal *H19* expression and results in reduced *Igf2* expression (Thorvaldsen et al., 1998; Thorvaldsen et al., 2002), to exclude the influence of paternal *H19* expression on the development of SC embryos, we attempted to remove the 13-kb region of *H19* that includes the gene body and the DMR in AG-haESCs (AGH-OG3) (Figure 5A, Figure S5A in Supporting Information). Two stable cell lines ($H19^{\triangle 13kb}$-AGH-OG3-1 and 2) were generated and shown to harbor an abnormal methylation status at *IG*-DMR similar to AGH-OG3 cells (Figure S5B and C in Supporting Information). ICAHCI analysis showed that $H19^{\triangle 13kb}$ led to comparable developmental potential of SC to DKO AG-haESCs (Figure 5B) on E12.5, probably through rescue of placental defects (Figure 5C–F, Figure S5D and E in Supporting Information). The expression of imprinted genes in $H19^{\triangle 13kb}$ placentas was similar to those in $H19^{\triangle DMR}$-$IG^{\triangle DMR}$ DKO placentas (Figure 5G). Interestingly, we observed fewer abnormal embryos in $H19^{\triangle 13kb}$ group compared to DKO group on E12.5 (Figure 5B), probably due to a slightly higher level of *Igf2* expression in $H19^{\triangle 13kb}$ embryos (Figure 5G).

We next checked the developmental potential of $H19^{\triangle 13kb}$ SC fetuses at late-gestation. Compared to DKO SC embryos, the percentage of $H19^{\triangle 13kb}$ SC embryos which normally developed to E18.5 was significantly reduced, accompanied with higher frequency of embryonic degeneration (Figure 5H). Interestingly, the surviving $H19^{\triangle 13kb}$ SC embryos showed higher fetal and placental weights compared to DKO embryos (Figure 5I). Notably, we observed that the DNA methylation at *IG*-DMR was normal in live SC pups but was lost in all abnormal $H19^{\triangle 13kb}$ embryos on E18.5 (Figure 5J and K, Figure S6A in Supporting Information). Furthermore, $H19^{\triangle 13kb}$ SC embryos with low methylation of *IG*-DMR were growth-retarded (Figure S6A and B in Supporting Information), and exhibited enhanced *Gtl2* expression but repressed *Dlk1* and *Dio3* expression in different tissues (Figure S6C in Supporting Information). Taken together, these results indicate the critical roles of the *Dlk1-Dio3* imprinted cluster in late-gestation development of SC embryos.

$H19^{\Delta 13kb}$ rescues developmental defects of SC embryos at mid-gestation through correction of placental defects

Since different deletions resulted in different phenotypes in placentas of E12.5, we then sought to explore whether de-

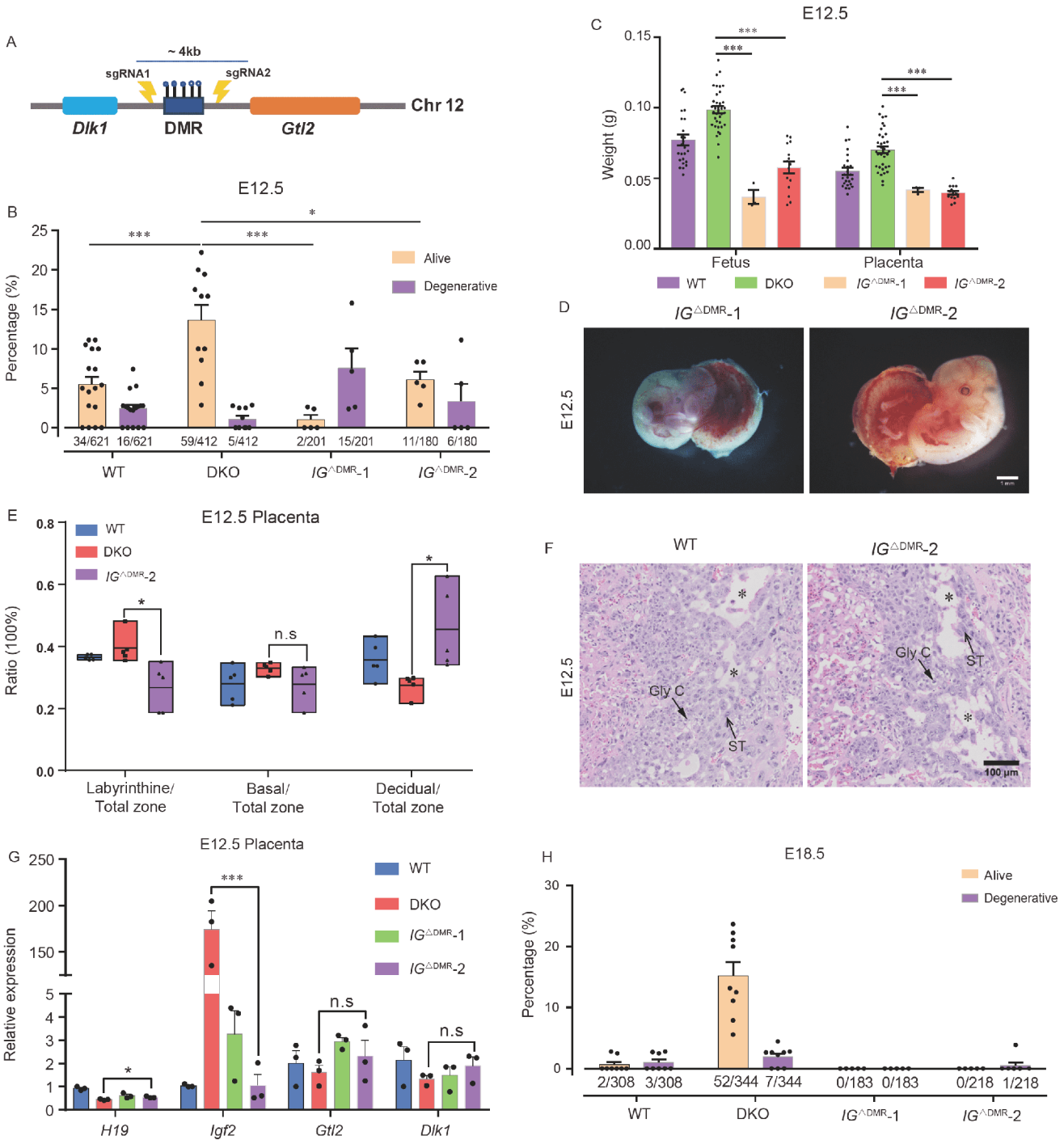

Figure 4 Deletion of *IG*-DMR alone fails to rescue the developmental retardation of SC embryos before E12.5. A, Schematic diagram of sgRNAs targeting for the removal of *IG*-DMR. A dark blue bar represents the deleted region (about 4 kb). B, The ratios of alive and degenerative SC embryos (E12.5) to transferred 2-cell embryos derived from WT (n=17 recipients), DKO (n=11 recipients) and $IG^{\triangle DMR}$ (n=5 recipients for each cell line) AG-haESCs. Numbers under the bars indicate E12.5 embryos/transferred two-cell embryos. C, The fetal and placental weights of E12.5 embryos derived from WT (n=25), DKO (n=36) and $IG^{\triangle DMR}$ (n=5 for $IG^{\triangle DMR}$-1 and n=15 for $IG^{\triangle DMR}$-2) AG-haESCs, showing severe retardation in $IG^{\triangle DMR}$ SC embryos compared with DKO. D, Severe growth-retardation shown in $IG^{\triangle DMR}$ SC fetuses (E12.5). Experiments were repeated five times independently, with similar results. E, The ratios of labyrinthine zone, basal zone and decidual zone to total placental areas of WT, DKO and $IG^{\triangle DMR}$ placentas (E12.5), indicating decreased labyrinthine zone and increased decidual area in $IG^{\triangle DMR}$ placentas compared with DKO, n=5 placentas for each group and at least 5 sections per placenta analyzed. Black lines are shown as the mean. F, Histological sections of the placentas from WT and $IG^{\triangle DMR}$ SC fetus on E12.5. Asterisks show vacuolation in WT and $IG^{\triangle DMR}$ placentas. Gly C, glycogen cells; ST, spongiotrophoblast. Experiments were repeated five times independently, with similar results. G, Transcriptional analysis of *H19*, *Igf2*, *Gtl2* and *Dlk1* genes in WT, DKO and $IG^{\triangle DMR}$ placentas (n=3 placentas for each group). The expression values were normalized to that of *Gapdh*. H, The ratios of alive and degenerative SC embryos (E18.5) to transferred 2-cell embryos derived from WT (n=8 recipients), DKO (n=9 recipients) and $IG^{\triangle DMR}$ (n=5 recipients for each cell lines) AG-haESCs. Numbers under the bars indicate E18.5 embryos/transferred two-cell embryos. Data are shown as the average mean±SEM in B, C, G and H. *, P<0.05; ***, P<0.001; n.s, no significant difference.

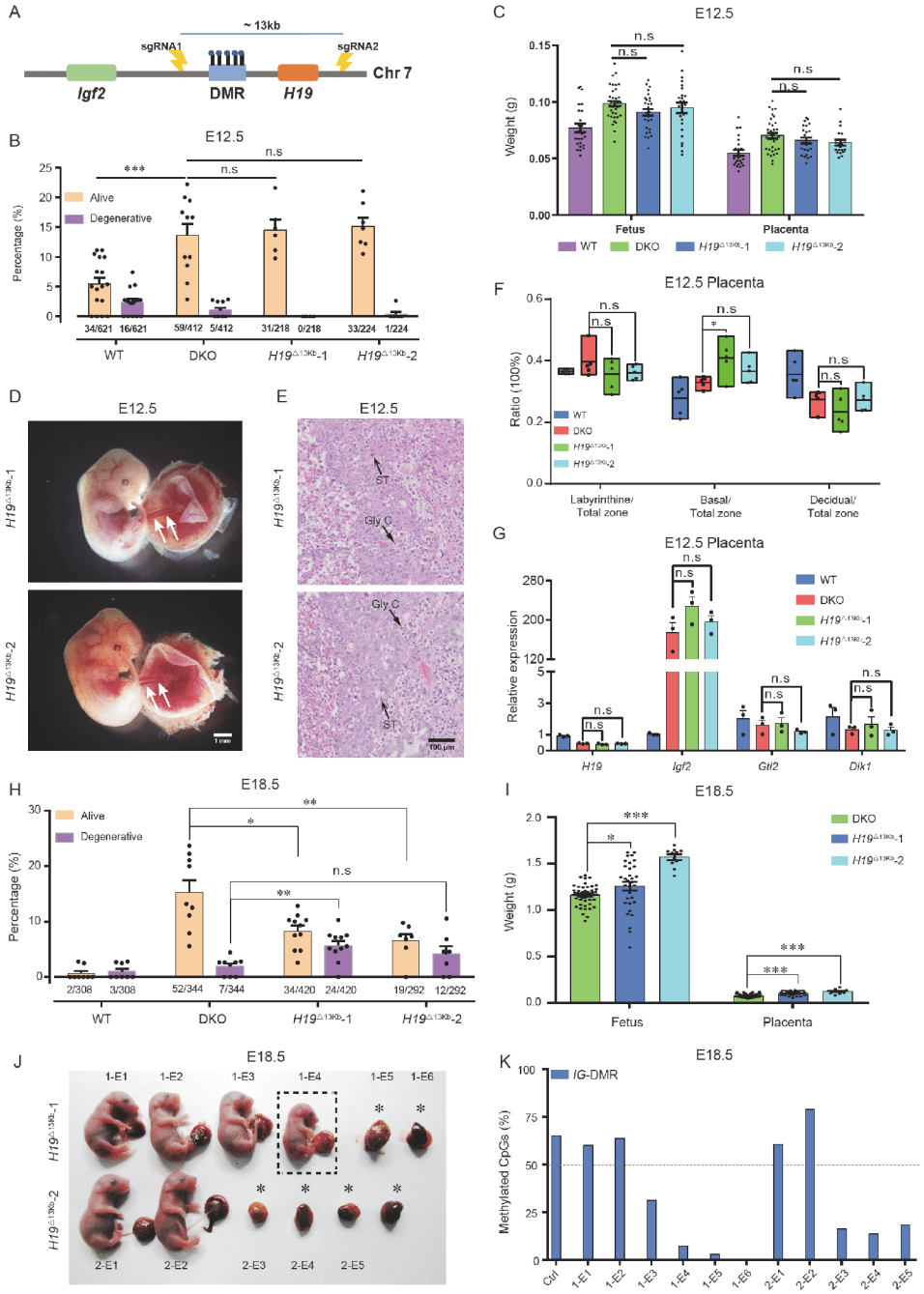

Figure 5 $H19^{\triangle 13kb}$ rescues the abnormal development of SC embryos at mid-gestation. A, Schematic diagram of sgRNAs targeting for the removal of *H19*-DMR and *H19* transcription unit (about 13 kb). B, The ratios of E12.5 alive and degenerative SC embryos to transferred 2-cell embryos derived from WT (n=17 recipients), DKO (n=11 recipients) and $H19^{\triangle 13kb}$ (n=6 recipients for $H19^{\triangle 13kb}$-1 and n=7 for $H19^{\triangle 13kb}$-2) AG-haESCs. Numbers under the bars indicate E12.5 embryos/transferred two-cell embryos. C, The fetal and placental weights of E12.5 SC embryos derived from WT (n=25), DKO (n=36) and $H19^{\triangle 13kb}$ (n=27 for $H19^{\triangle 13kb}$-1 and n=25 for $H19^{\triangle 13kb}$-2) AG-haESCs, showing comparable developmental potential of $H19^{\triangle 13kb}$ and DKO SC embryos. D, Images of $H19^{\triangle 13kb}$ SC fetuses (E12.5) showing normal development. White arrows show the umbilical cords. Experiments were repeated five times independently, with similar results. E, Histological sections of the placentas from $H19^{\triangle 13kb}$ SC fetus on E12.5. Gly C, glycogen cells; ST, spongiotrophoblast. Experiments were repeated five times independently, with similar results. F, The ratios of labyrinthine zone, basal zone and decidual zone to total placental areas of WT, DKO and $H19^{\triangle 13kb}$ placentas (E12.5), indicating comparable development of DKO and $H19^{\triangle 13kb}$ placentas. n=5 placentas for each group and at least 5 sections per placenta were analyzed. Black lines are shown as the mean. G, Transcriptional analysis of *H19*, *Igf2*, *Gtl2* and *Dlk1* genes in WT, DKO and $H19^{\triangle 13kb}$ placentas (n=3 placentas for each group). The expression values were normalized to that of *Gapdh*. H, The ratios of alive and degenerative SC embryos (E18.5) to transferred 2-cell embryos derived from WT (n=8 recipients), DKO (n=9 recipients) and $H19^{\triangle 13kb}$ (n=11 recipients for $H19^{\triangle 13kb}$-1 and n=7 for $H19^{\triangle 13kb}$-2) AG-haESCs. Numbers under the bars indicate E18.5 embryos/transferred two-cell embryos. I, The fetal and placental weights of E18.5 SC embryos derived from DKO (n=51) and $H19^{\triangle 13kb}$ (n=32 for $H19^{\triangle 13kb}$-1 and n=11 for $H19^{\triangle 13kb}$-2) AG-haESCs. Data are shown as the average mean ±SEM in B, C and G–I. *, P<0.05; **, P<0.01; ***, P<0.001; n.s, no significant difference. J and K, Images of $H19^{\triangle 13kb}$ SC embryos on E18.5 (J) and their methylation state at the *IG*-DMR (K). The black dotted box shows a retarded embryo and asterisks show degenerative embryos. The dotted line in (K) shows theoretical value of methylation (50%).

letions changed gene expression in the placenta by performing RNA sequencing (RNA-seq) analysis. To do this, we collected E12.5 placentas of five groups (three replicates for each group) derived from sperm (ICSI), WT AG-haESCs (WT), $H19^{\triangle DMR}$-$IG^{\triangle DMR}$-AG-haESCs (DKO), $IG^{\triangle DMR}$-AG-haESCs ($IG^{\triangle DMR}$) and $H19^{\triangle 13kb}$-AG-haESCs ($H19^{\triangle 13kb}$). The results indicated that transcriptomes of WT and $IG^{\triangle DMR}$ placentas were clearly clustered together and exhibited patterns different from ICSI, $H19^{\triangle 13kb}$ and DKO placentas (Figure 6A, Figure S7A and B in Supporting Information). These results were consistent with the observations that $H19^{\triangle 13kb}$ and DKO significantly rescued the placental defects, while $IG^{\triangle DMR}$ showed severe placental defects similar to WT (Figures 4C–F and 5C–F). We further compared the expression patterns of imprinted genes and found that two groups of such genes were differentially expressed between DKO/$H19^{\triangle 13kb}$/ICSI and $IG^{\triangle DMR}$/WT, including genes involved in *H19-Igf2* and *Dlk1-Dio3* imprinted clusters (Figure 6B and C). Moreover, we also found three classes of genes which showed differential expression levels among the five groups of placentas (Figure 6D). Class I (n=64) with lower expression in $IG^{\triangle DMR}$/WT compared to DKO/$H19^{\triangle 13kb}$/ICSI was associated with the cell cycle; Class II (n=137) with higher expression in $IG^{\triangle DMR}$/WT was enriched for developmental genes; Class III (n=55), specifically expressed in WT, was mainly associated with chromatin assembly (Figure 6D and E). Interestingly, we noticed that some *Hox* genes were abnormally activated in $IG^{\triangle DMR}$/WT (Figure 6F). A previous study has shown that *H19* and *Igf2* are inactive during the first cell fate decision (ICM and TE formation), while they are specifically activated in visceral endoderm (VE) cells that mainly contribute to placental development, but not in epiblast (Epi) cells that develop into embryonic tissues (Figure 6G) (Zhang et al., 2018). These observations suggest that *H19* and *H19*-DMR may play a role in repression of development-related genes in placentas. In summary, $IG^{\triangle DMR}$ cannot rescue the abnormal gene expression in WT, including imprinted genes and other functional genes in E12.5 placentas, which may lead to severe developmental defects of SC embryos. In contrast, DKO and $H19^{\triangle 13kb}$ correct the misexpression of genes in placentas, which contributes to the normal development in placentas. Taken together, these results indicated that the *H19-Igf2* locus on the paternal genome plays a key role in the SC embryonic development before mid-gestation, whereas the *Dlk1-Dio3* locus on the paternal genome is indispensable for normal embryonic development of late-gestation.

Triple deletions of *H19*, *H19*-DMR and *IG*-DMR further improve the developmental potential of SC embryos

Given that $H19^{\triangle 13kb}$ can give rise to better development compared to the DKO group on E12.5 (Figure 5B), we asked whether combined deletions of $H19^{\triangle 13kb}$ (including *H19* and *H19*-DMR) and *IG*-DMR (TKO-AG-haESCs) could further improve full-term developmental potential of SC embryos. Two stable cell lines were generated through removal of *IG*-DMR in $H19^{\triangle 13kb}$-AGH-OG3-1 (termed $H19^{\triangle 13kb}$-$IG^{\triangle DMR}$-AGH-OG3-1 and 2 or TKO-1 and 2) and injected into oocytes to produce mice (Figure 7A and B, Figure S8A and B in Supporting Information). The results showed that TKO-1 exhibited comparable developmental efficiency on E18.5 to that of DKO cells, while TKO-2 cells displayed a significantly higher efficiency (Figure 7B). Interestingly, TKO SC embryos exhibited remarkably higher body and placental weights than those of DKO conceptuses, reaching the levels of the ICSI group (Figure 7C and D). These phenotypes could be caused by total deletion of paternal *H19*, resulting in decreased *H19* expression in major organs during embryonic development (Figure 7E).

Importantly, the birth rate and body weight of TKO-2 newborn pups were notably higher than those of the DKO (Figure 7F–H). Furthermore, growth profiling analysis showed that TKO-2 enhanced the postnatal growth of SC mice (Figure 7I). Furthermore, removal of the *H19* gene-body in another DKO cell line (termed $H19^{\triangle DMR}$-$IG^{\triangle DMR}$-AGH-2 or O48) generated previously (Zhong et al., 2015) resulted in a stable cell line termed O48-TKO, from which, SC pups with higher birth weight were produced (Figure S8C–E in Supporting Information). Finally, we tested the reproductive ability of TKO SC mice by collecting mature oocytes from super-ovulated 4-week-old SC mice. The average number of oocytes from each mouse was similar among TKO, DKO and ICSI groups (Figure S8F and G in Supporting Information). In addition, the concentration of luteinizing hormone (LH) in the plasma of adult mice (4 months old) was also comparable between SC and control mice (Figure S8H in Supporting Information). Moreover, TKO mice grew to adulthood and reproduced normally (Figure S8I in Supporting Information). Genotyping analysis of a total of 9 live-born pups from 2 litters of progeny delivered by TKO SC mice showed that 3 pups carried the 13 kb-deletion of *H19* (Figure S8J in Supporting Information). All pups harboring the maternal deletion of *IG*-DMR died shortly after birth, consistent with previous reports that maternal transmission of the *IG*-DMR deletion causes postnatal or neonatal lethality (Lin et al., 2003; Zhong et al., 2015). Taken together, these results indicated that the TKO can further improve prenatal and postnatal development of SC embryos.

DISCUSSION

Previous studies have shown that ng oocytes carrying both *H19*-DMR and *IG*-DMR can efficiently support bi-maternal

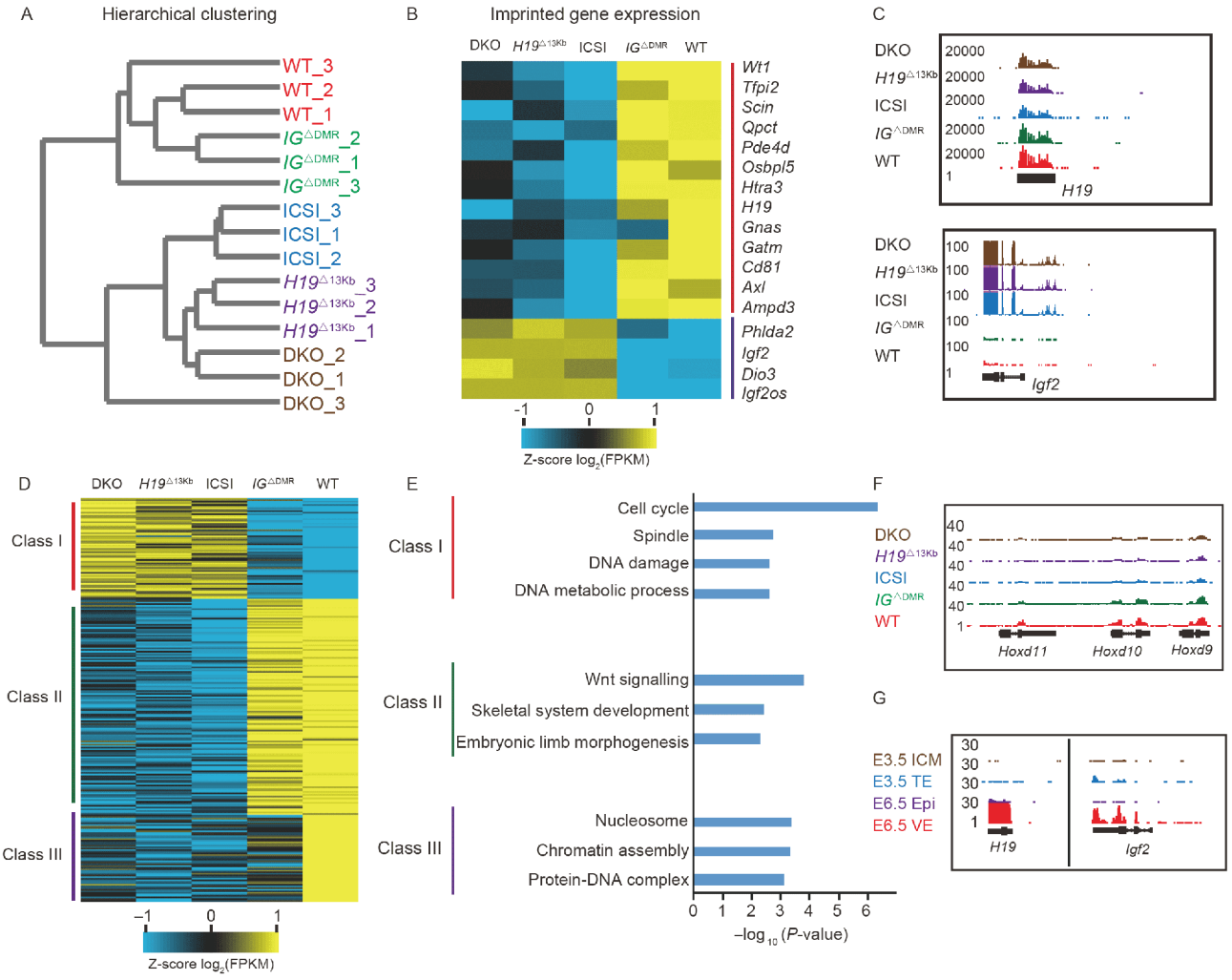

Figure 6 Global transcriptome analysis of SC placentas with different DNA/gene deletions. A, The hierarchical clustering analysis of RNA dataset from placentas obtained through oocyte injection of sperm, WT, $IG^{\triangle DMR}$, $H19^{\triangle 13kb}$ and DKO AG-haESCs respectively. B, Differentially expressed imprinted genes in different placentas. Representative genes enriched in each cluster are shown in the right column. C, UCSC Genome Browser (University of California, Santa Cruz) snapshots of *H19* and *Igf2* expression levels in different placentas. D and E, The heatmap showing 3 classes of differentially expressed genes among different placentas (D) and Gene Ontology (GO) analysis of genes in the 3 classes (E). F, Genome Browser snapshots of *Hoxd11*, *Hoxd10* and *Hoxd9* expression levels in different placentas. G, Genome Browser snapshots of *H19* and *Igf2* expression levels in E3.5 and E6.5 embryos, according to previous data (Zhang et al., 2018).

embryonic development after fusion with a mature oocyte (Kawahara et al., 2007). Meanwhile, we showed that removal of these two DMRs in AG and PG-haESCs can result in high-efficiency generation of SC and bi-maternal mice respectively through injection into oocytes (Zhong et al., 2016; Zhong et al., 2015). Moreover, we found that *H19*-DMR and *IG*-DMR deletions do not change the transcriptional and methylation profiles in haESCs (Zhong et al., 2016; Zhong et al., 2015), implying that *H19*-DMR and *IG*-DMR may function during embryonic development after injection of haploid cells into oocytes. However, it is still largely unknown how *H19*-DMR and *IG*-DMR coordinately regulate SC embryonic development. In this study, we show that *H19*-DMR and *IG*-DMR temporally regulate SC embryo development (Figure 7J). *H19*-DMR and *IG*-DMR are dispensable for the pre-implantation development of SC embryos. *H19*-DMR is indispensable for mid-gestation development, while *IG*-DMR plays a critical role in late-gestation development. *H19*-DMR is important for placental development before mid-gestation and double deletions of *H19* and *H19*-DMR further improve SC embryonic development at mid-gestation, probably through regulation of *Igf2* expression. Importantly, triple knockout of *H19*, *H19*-DMR and *IG*-DMR further improve the prenatal and postnatal development of SC mice.

Mice carrying paternal *H19*-DMR or *IG*-DMR deletion that partially mimic the methylation state of DMR (Barlow and Bartolomei, 2014) were generated more than a decade ago (Lin et al., 2003; Thorvaldsen et al., 2002), displaying minimal if any adverse phenotypes. Therefore, it is expected

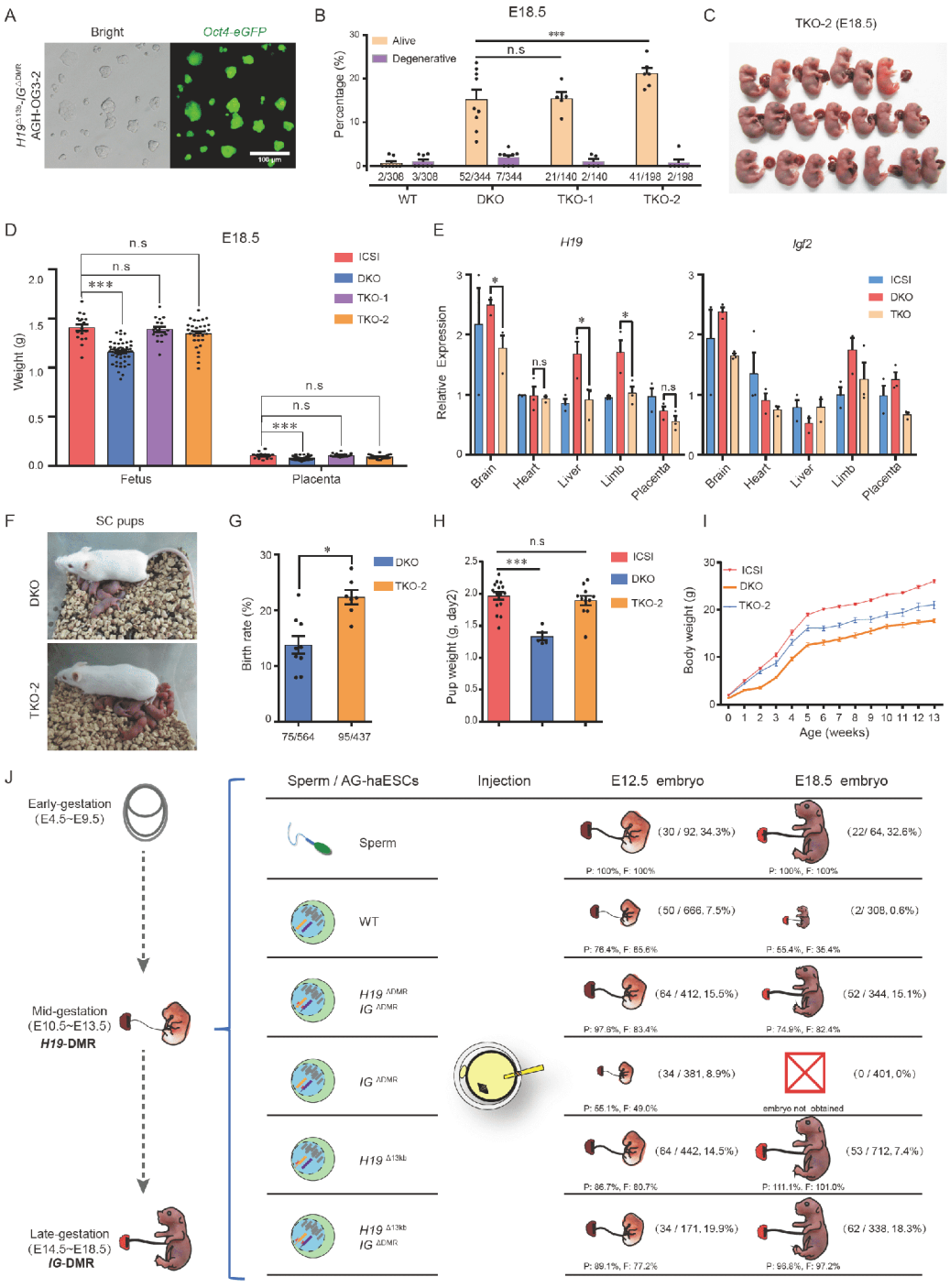

Figure 7 Combined deletion of *H19*, *H19*-DMR and *IG*-DMR in AG-haESCs further increases the prenatal and postnatal development of SC embryos. A, Images of a TKO-AG-haESC ($H19^{\triangle 13kb}$-$IG^{\triangle DMR}$-AGH-OG3-2) line carrying an *Oct4-eGFP* transgene. B, The ratios of alive and degenerative E18.5 SC embryos to transferred 2-cell embryos derived from WT (n=8 recipients), DKO (n=9 recipients) and TKO (n=5 recipients for TKO-1 and 6 for TKO-2) AG-haESCs. Numbers under the bars indicate E18.5 embryos/transferred two-cell embryos. C, E18.5 TKO SC pups derived from TKO-2 cells. Experiments were repeated three times independently, with similar results. D, The fetal and placental weights of E18.5 embryos derived from sperm (n=17), DKO (n=51) and TKO (n=19 for TKO-1 and n=32 for TKO-2) AG-haESCs, showing comparable development of TKO SC and control embryos (ICSI). E, Transcriptional analysis of imprinted genes *H19* and *Igf2* in different tissues of E18.5 fetuses (ICSI, DKO and TKO), including brain, heart, liver, limb and placenta (n=3 samples for each group). The expression values were normalized to that of *Gapdh*. F and G, The birth rates of SC pups from ICAHCI experiments using DKO and TKO-2 cells (G). Representative images of recipient mouse and SC pups shown in (F). H, Higher body weight of TKO-2 SC pups than that of DKO pups on postnatal day 2. I, Growth curve of ICSI (females, n=9), DKO (n=4) and TKO-2 SC mice (n=10), showing that TKO improves the postnatal developmental potential of SC mice. Data are shown as the average mean±SEM in B, D, E and G–I. *, P<0.05; ***, P<0.001; n.s, no significant difference. J, Summary of the temporal regulation of paternal genomic imprinting (*H19*-DMR and *IG*-DMR) during SC embryonic development. The percentages of placental (P) and fetal (F) weights are based on the placental and fetal weights of ICSI. The numerator in parentheses represents the alive embryos obtained and denominator represents the total number of transferred two-cell embryos.

that sperm with both *H19*-DMR and *IG*-DMR deletions obtained through multiple rounds of breeding between two mutant mouse lines may also result in overall normal embryonic development, thus impeding the study of coordinated regulation between two imprinted loci in embryonic development. In contrast, AG-haESCs with low methylation level especially in imprinted regions result in abnormal embryonic development upon injection into oocytes (Yang et al., 2012). Interestingly, after removal of *H19*-DMR and *IG*-DMR in AG-haESCs to rescue the methylation loss at DMRs, the resultant DKO-AG-haESCs can efficiently support normal SC embryonic development, leading to live pups with a high birth rate comparable to that of round spermatid injection (ROSI) (Zhong et al., 2015). Taken together, these results suggest that AG-haESCs, acting as the sperm replacement, can be used to study the imprinting function *in vivo*. Using this technology, our current study reveals the temporal regulation of prenatal embryonic development by paternal *H19-Igf2* and *Dlk1-Dio3*, providing strong evidence to demonstrate AG-haESCs as a unique tool to study genomic imprinting *in vivo* (Li and Li, 2019).

Due to the accessibility of genomic modifications in AG-haESCs, this technology may be extended to different aspects of imprinting studies *in vivo*, such as (1) identification of maternal imprinted genes that are critical for embryonic development, whose deletion in AG-haESCs may result in SC embryonic lethality; (2) investigation of control elements of the imprinted locus through one-step generation of SC mice carrying different modifications in the imprinted locus by respective injection of AG-haESCs with corresponding mutations into oocytes; (3) characterization of the expression pattern of an imprinted gene during embryonic development through insertion of a standard tag endogenously in AG-haESCs; and (4) interaction analysis between different imprinted genes/loci.

TKO-AG-haESCs generated in this study exhibit higher developmental potential and better postnatal development of SC embryos; these cell types, combined with CRISPR-Cas9 technology, may enhance genetic analyses *in vivo* (Li et al., 2018; Wang and Li, 2019; Wei et al., 2017; Yan and Li, 2019). Further investigation into *H19-Igf2*, *Dlk1-Dio3* or other loci will not only reveal mechanisms involved in embryonic development but may also help to fine-tune embryonic development for more efficient generation of SC mice.

MATERIALS AND METHODS

Animals

All mice were housed in individual ventilated cages (IVC) under specific-pathogen-free conditions and a 12:12 h light/dark cycle. MII oocytes are all from B6D2F1 (C57BL/6♀×DBA/2♂) female mice. The *Oct4-eGFP* males (C57BL/6 background) provided sperm for ICSI experiments. All the pseudopregnant foster mothers were ICR females. All animal procedures were performed under the ethical guidelines of the Shanghai Institute of Biochemistry and Cell Biology, Chinese Academy of Sciences, Shanghai, China.

Plasmid construction

To generate CRISPR-Cas9 plasmid for gene manipulation, specific sgRNAs were synthesized (Sunya, Shanghai), annealed, and fused to BpiI (Thermo Fisher Scientific, USA)-linearized pX330-*mCherry* plasmid (Addgene#98750) (Wu et al., 2013). All inserted sgRNA sequences were validated by Sanger sequencing.

Cell culture and transfection

Mouse androgenetic haploid embryonic stem cells (AG-haESCs) of AGH-OG3 and *H19*$^{\triangle DMR}$-*IG*$^{\triangle DMR}$-AGH-OG3 were from our previous work (Yang et al., 2012; Zhong et al., 2015), respectively. These cells were cultured in DMEM (Merk, Germany) with 15% FBS (Thermo Fisher Scientific, USA), Penicillin-Streptomycin, Non-Essential Amino Acids, Nucleosides, L-Glutamine Solution, 2-Mercaptoethanol, 1,000 U mL^{-1} Lif, 1 μmol L^{-1} PD03259010 (Selleck, USA) and 3 μmol L^{-1} CHIR99021 (Selleck, USA). Cells were transfected using Lipofectamine 3000 reagent (Thermo Fisher Scientific, USA) according to the manufacturer's protocols.

CRISPR/Cas9 mediated imprinted region deletion

For construction of gene-edited AG-haESCs, cells were transfected with corresponding pX330-*mCherry* plasmids, including specific sgRNAs (Table S1 in Supporting Information). 24 h after transfection, the haploid cells expressing red fluorescence protein were enriched with flow cytometry (FACS AriaII, BD Biosciences, USA) and plated at low density (about 8,000 cells per well of a 6-well plate). One week after plating, a single colony was picked for derivation of gene manipulation AG-haESCs identified by PCR and Sanger sequencing. For the enrichment of haploid cells, cells were treated with trypsin, incubated with 15 μg mL^{-1} Hoechst 33342 (Thermo Fisher Scientific, USA) in 37°C water bath for 5–10 min, transferred through a 40-μm cell strainer and enriched by sorting 1N peak of DAPI channel on AriaII.

Genomic DNA extraction and genotyping

Mouse tails and AG-haESCs were lysed by Mouse Direct PCR Kit (Bimake, USA) according to the manufacturer's

guidance. After centrifuge, 12,000 r min^{-1} for 10 min, 1–2 μL supernatant of digested solution was used as the PCR template. The genome extraction from mouse embryos or pups used the TIANamp Genomic DNA Kit (TIANGEN, China) for genotyping or bisulphite sequencing.

Bisulphite sequencing

The bisulfite conversion was performed in one-step using the EZ DNA Methylation-GoldTM Kit (ZYMO research, USA) for 500 ng genomic DNA, following the manufacturer's instructions. The recovered DNA products were amplified by a first round of nested PCR, followed by a second round using loci specific PCR primers (Table S1 in Supporting Information). The amplified products were purified by gel electrophoresis using Universal DNA Purification Kit (TIANGEN, China) and cloned into pEASY-Blunt vector (TransGen Biotech, China). For each sample, more than 15 *E. coli* clones were picked for sequencing. The results were analyzed by DNA methylation analysis platform (http://services.ibc.uni-stuttgart.de/BDPC/BISMA/).

RNA extraction and quantitative real-time PCR

Total RNA was isolated from cells and tissues of embryos (E8.5, E9.5, E12.5 and E18.5) using TRIzol™ Reagent (Thermo Fisher Scientific, USA). To synthesize cDNAs for real-time PCR, 500 ng of total RNA was directly used as the template with ReverTra Ace® qPCR RT Master Mix (TOYOBO, Japan). To obtain RNA from embryos with low-cell number (E3.5, E6.5 and E7.5), samples were lysed in 150 μL of 4 mol L^{-1} guanidine isothiocyanate solution (Thermo Fisher Scientific, USA) at 42°C for 10 min. Total RNA pellets were concentrated by UltraPure™ Glycogen (Thermo Fisher Scientific, USA). To get enough template for real-time PCR, two rounds of amplification were performed according to a reported protocol (Chen et al., 2017). Quantitative real-time PCR was performed on a Bio-Rad CFX96 instrument using SYBR® qPCR Mix (TOYOBO, Japan) in triplicate. All gene expression was calculated based on the $2^{-\Delta\Delta Ct}$ method after normalization to the transcript level of the internal standard gene, *Gapdh* (ID: 14433). All the primer sequences are listed in Table S1 in Supporting Information.

RNA sequencing and analyzing

To separate ICM and TE from E3.5 embryos (Liu et al., 2016), blastocysts were broken using micromanipulator and washed three times in HCZB. The zona pellucidae of blastocysts were digested with 0.5% pronase E (Sigma, USA) for 10–15 min and washed three times again in HCZB. The embryos were then incubated in Ca^{2+}-free CZB for 30 min in 37°C, and the ICM and TE were separated into single cells by gently pipetting using a pipette with a diameter of 40–60 μm. Each sample was obtained about 10 cells from one embryo for amplification according to the cell shape. ICM cells are small and out-of-shape, while TE cells are large and smooth. The cDNAs of low-input cells were harvested according to previous protocols (Picelli et al., 2014). The cDNA libraries were prepared by SPAPK DNA Sample Pre Kit (Enzymatics, Germany) for sequencing using an Illumina HiSeq X Ten sequenator. Total RNA was isolated from mouse placentas using a Dynabeads™ mRNA DIRECT™ Purification Kit (Thermo Fisher Scientific, USA). RNA-seq libraries were prepared by VAHTS mRNA-seq V3 Library Prep Kit for Illumina® (Vazyme, China), and then subjected to deep sequencing on Illumina NovaSeq6000 platform. All RNA-seq reads were mapped to mm9 with TopHat (version 2.2.1). The mapped reads were further analyzed by Cufflinks, and the expression levels for each transcript were quantified as Fragments Per Kilobase of transcript per Million mapped reads (FPKM).

Intracytoplasmic AG-haESC or sperm injection

To generate SC embryos, AG-haESC clones were treated with 0.05 μg mL^{-1} Demecolcine solution (Sigma, USA) for 10–12 h and synchronized to M phase. These clones were treated with trypsin and suspended in HCZB medium. MII oocytes were collected from oviducts of superovulated B6D2F1 females (8 weeks old). AG-haESCs were injected into the cytoplasm of MII oocytes in a droplet of HCZB medium containing 5 μg mL^{-1} cytochalasin B (Sigma, USA) using a Piezo-drill micromanipulator. The reconstructed oocytes were cultured in CZB medium for 30 min and then activated for 5–6 h in Ca^{2+} free CZB with $SrCl_2$. For ICSI experiments, the procedures were the same as described above, except that AG-haESCs were replaced by sperm. Following activation, all of the reconstructed embryos were cultured for 24 h in AA-KSOM (Merk, Germany) medium at 37°C under 5% CO_2 in air.

Embryo transfer and cesarean section

Reconstructed embryos were cultured in AA-KSOM medium until the two-cell or blastocyst stage. Thereafter, 14–16 (for ICSI) and 18–20 (for ICAHCI) two-cell embryos were transferred into each oviduct of pseudopregnant ICR females at 0.5 days post copulation. The post-implantation embryonic development (from E6.5 to E18.5) was assessed by an autopsy, and the embryos were quickly removed from the uteri and photographed immediately. Some E12.5 and E18.5 embryos and placentas were weighed after being dried with absorbent paper.

Histology analysis of placentas

The placentas of E12.5 were fixed in 4% paraformaldehyde overnight at room temperature, dehydrated with gradient concentration of alcohol (50%, 60%, 70%, 80%, 95% and 100%, diluted with distilled water), and embedded in paraffin and sectioned. Serial sections (4 μm) prepared in the cross planes were mounted on slides and de-waxed in xylene and rehydrated in different concentration of alcohol (100%, 95%, 70% and 50%, diluted with distilled water), followed by staining with hematoxylin and eosin. In each placenta, five sections of different slides were picked up to calculate the total placenta area, decidual zone area, labyrinthine zone area, and basal zone area. The values were measured with ImageJ software, and the area is the average of five different sections of each sample.

Collection of mature oocytes and measure of luteinizing hormone (LH)

Control (ICSI), DKO and TKO female mice (4 weeks old) were superovulated with 4 international units of pregnant mare's serum gonadotropin (PMSG) for 48 h and then human chorionic gonadotropin (hCG) for 12 h. Mature oocytes were collected from ampulla of the fallopian tube after superovulation. Plasma was collected from 4-month-old female mice using heparin as an anticoagulant. All samples were centrifuged for 15 min at 1,000×*g* at 4°C within 30 min and the supernatant was collected for the next assay. LH signals were detected from plasma using Mouse LH/Luteinizing Hormone ELISA Kit (LSBio, USA), following the manufacturer's instructions.

Statistical analysis

For all figures, results shown are the average mean±standard error of the mean (SEM). Statistical testing was performed using GraphPad Prism 7. Significance was determined by two-tailed, unpaired Student's *t*-test. *, $P<0.05$; **, $P<0.01$; ***, $P<0.001$; n.s, no significant difference.

Data availability

The RNA sequencing data of blastocysts and placentas from this study have been deposited in the Gene Expression Omnibus (GEO) under accession number GSE132254. The RNA sequencing data of AGH-OG3 and *H19*$^{\triangle DMR}$-*IG*$^{\triangle DMR}$-AGH-OG3 obtained from our previous work under the accession number GSE60072. The RNA sequencing data of ICM and TE of E3.5 and Epi and VE of E6.5 from previous work under the accession number GSE76505. All other data supporting the findings of this study are available from the corresponding author on reasonable request.

Compliance and ethics *The author(s) declare that they have no conflict of interest.*

Acknowledgements *This work was partly supported by the Genome Tagging Project, Fountain-Valley Life Sciences Fund of University of Chinese Academy of Sciences Education Foundation and grants from the Chinese Academy of Sciences (XDB19010204, OYZDJ-SSW-SMC023 and Facility-based Open Research Program), the National Natural Science Foundation of China (31530048, 81672117, 31730062, 31821004, and 31601163), the Ministry of Science and Technology of China (2019YFA0109900), and Shanghai Municipal Commission for Science and Technology (16JC1420500, 17JC1420102, 17JC1400900, and 17411954900).*

References

Angiolini, E., Coan, P.M., Sandovici, I., Iwajomo, O.H., Peck, G., Burton, G.J., Sibley, C.P., Reik, W., Fowden, A.L., and Constância, M. (2011). Developmental adaptations to increased fetal nutrient demand in mouse genetic models of Igf2-mediated overgrowth. FASEB J 25, 1737–1745.
Arney, K.L. (2003). H19 and Igf2—enhancing the confusion? Trends Genets 19, 17–23.
Barlow, D.P., and Bartolomei, M.S. (2014). Genomic imprinting in mammals. Cold Spring Harb Perspect Biol 6.
Bartolomei, M.S., Zemel, S., and Tilghman, S.M. (1991). Parental imprinting of the mouse H19 gene. Nature 351, 153–155.
Bell, A.C., and Felsenfeld, G. (2000). Methylation of a CTCF-dependent boundary controls imprinted expression of the *Igf2* gene. Nature 405, 482–485.
Bell, A.C., West, A.G., and Felsenfeld, G. (1999). The protein CTCF is required for the enhancer blocking activity of vertebrate insulators. Cell 98, 387–396.
Brunkow, M.E., and Tilghman, S.M. (1991). Ectopic expression of the *H19* gene in mice causes prenatal lethality.. Genes Dev 5, 1092–1101.
Burns, J.L., and Hassan, A.B. (2001). Cell survival and proliferation are modified by insulin-like growth factor 2 between days 9 and 10 of mouse gestation. Development 128, 3819.
Chen, J., Suo, S., Tam, P.P., Han, J.D.J., Peng, G., and Jing, N. (2017). Spatial transcriptomic analysis of cryosectioned tissue samples with Geo-seq. Nat Protoc 12, 566–580.
Choi, J., Huebner, A.J., Clement, K., Walsh, R.M., Savol, A., Lin, K., Gu, H., Di Stefano, B., Brumbaugh, J., Kim, S.Y., et al. (2017). Prolonged Mek1/2 suppression impairs the developmental potential of embryonic stem cells. Nature 548, 219–223.
Cleaton, M.A.M., Edwards, C.A., and Ferguson-Smith, A.C. (2014). Phenotypic outcomes of imprinted gene models in mice: elucidation of pre- and postnatal functions of imprinted genes. Annu Rev Genom Hum Genet 15, 93–126.
Constância, M., Angiolini, E., Sandovici, I., Smith, P., Smith, R., Kelsey, G., Dean, W., Ferguson-Smith, A., Sibley, C.P., Reik, W., et al. (2005). Adaptation of nutrient supply to fetal demand in the mouse involves interaction between the *Igf2* gene and placental transporter systems. Proc Natl Acad Sci USA 102, 19219–19224.
Constância, M., Hemberger, M., Hughes, J., Dean, W., Ferguson-Smith, A., Fundele, R., Stewart, F., Kelsey, G., Fowden, A., Sibley, C., et al. (2002). Placental-specific IGF-II is a major modulator of placental and fetal growth. Nature 417, 945–948.
DeChiara, T.M., Efstratiadis, A., and Robertson, E.J. (1990). A growth-deficiency phenotype in heterozygous mice carrying an insulin-like growth factor II gene disrupted by targeting. Nature 345, 78–80.
DeChiara, T.M., Robertson, E.J., and Efstratiadis, A. (1991). Parental imprinting of the mouse insulin-like growth factor II gene. Cell 64, 849–859.
Eggenschwiler, J., Ludwig, T., Fisher, P., Leighton, P.A., Tilghman, S.M., and Efstratiadis, A. (1997). Mouse mutant embryos overexpressing IGF-II exhibit phenotypic features of the Beckwith-Wiedemann and Simpson-Golabi-Behmel syndromes. Genes Dev 11, 3128–3142.

Ferguson-Smith, A.C. (2011). Genomic imprinting: the emergence of an epigenetic paradigm. Nat Rev Genet 12, 565–575.
Graham, C.F. (1970). Parthenogenetic mouse blastocysts. Nature 226, 165–167.
Hark, A.T., Schoenherr, C.J., Katz, D.J., Ingram, R.S., Levorse, J.M., and Tilghman, S.M. (2000). CTCF mediates methylation-sensitive enhancer-blocking activity at the H19/Igf2 locus. Nature 405, 486–489.
Jiang, J., Yan, M., Li, D., and Li, J. (2019). Genome tagging project: tag every protein in mice through 'artificial spermatids'. Natl Sci Rev 6, 394–396.
Kaufman, M.H. (1973). Parthenogenesis in the mouse. Nature 242, 475–476.
Kawahara, M., Wu, Q., Takahashi, N., Morita, S., Yamada, K., Ito, M., Ferguson-Smith, A.C., and Kono, T. (2007). High-frequency generation of viable mice from engineered bi-maternal embryos. Nat Biotechnol 25, 1045–1050.
Kobayashi, S., Fujihara, Y., Mise, N., Kaseda, K., Abe, K., Ishino, F., and Okabe, M. (2010). The X-linked imprinted gene family Fthl17 shows predominantly female expression following the two-cell stage in mouse embryos. Nucleic Acids Res 38, 3672–3681.
Kono, T., Obata, Y., Wu, Q., Niwa, K., Ono, Y., Yamamoto, Y., Park, E.S., Seo, J.S., and Ogawa, H. (2004). Birth of parthenogenetic mice that can develop to adulthood. Nature 428, 860–864.
Kono, T., Obata, Y., Yoshimzu, T., Nakahara, T., and Carroll, J. (1996). Epigenetic modifications during oocyte growth correlates with extended parthenogenetic development in the mouse. Nat Genet 13, 91–94.
Kono, T., Sotomaru, Y., Katsuzawa, Y., and Dandolo, L. (2002). Mouse parthenogenetic embryos with monoallelic H19 expression can develop to day 17.5 of gestation. Dev Biol 243, 294–300.
Leighton, P.A., Ingram, R.S., Eggenschwiler, J., Efstratiadis, A., and Tilghman, S.M. (1995). Disruption of imprinting caused by deletion of the H19 gene region in mice. Nature 375, 34–39.
Li, Q., Li, Y., Yang, S., Huang, S., Yan, M., Ding, Y., Tang, W., Lou, X., Yin, Q., Sun, Z., et al. (2018). CRISPR–Cas9-mediated base-editing screening in mice identifies DND1 amino acids that are critical for primordial germ cell development. Nat Cell Biol 20, 1315–1325.
Li, W., Shuai, L., Wan, H., Dong, M., Wang, M., Sang, L., Feng, C., Luo, G.Z., Li, T., Li, X., et al. (2012). Androgenetic haploid embryonic stem cells produce live transgenic mice. Nature 490, 407–411.
Li, Y., and Li, J. (2019). Technical advances contribute to the study of genomic imprinting. PLoS Genet 15, e1008151.
Li, Z., Wan, H., Feng, G., Wang, L., He, Z., Wang, Y., Wang, X.J., Li, W., Zhou, Q., and Hu, B. (2016). Birth of fertile bimaternal offspring following intracytoplasmic injection of parthenogenetic haploid embryonic stem cells. Cell Res 26, 135–138.
Lin, S.P., Youngson, N., Takada, S., Seitz, H., Reik, W., Paulsen, M., Cavaille, J., and Ferguson-Smith, A.C. (2003). Asymmetric regulation of imprinting on the maternal and paternal chromosomes at the Dlk1-Gtl2 imprinted cluster on mouse chromosome 12. Nat Genet 35, 97–102.
Liu, W., Liu, X., Wang, C., Gao, Y., Gao, R., Kou, X., Zhao, Y., Li, J., Wu, Y., Xiu, W., et al. (2016). Identification of key factors conquering developmental arrest of somatic cell cloned embryos by combining embryo biopsy and single-cell sequencing. Cell Discov 2, 16010.
Lopez, M.F., Dikkes, P., Zurakowski, D., and Villa-Komaroff, L. (1996). Insulin-like growth factor II affects the appearance and glycogen content of glycogen cells in the murine placenta.. Endocrinology 137, 2100–2108.
McGrath, J., and Solter, D. (1984). Completion of mouse embryogenesis requires both the maternal and paternal genomes. Cell 37, 179–183.
Morrione, A., Valentinis, B., Xu, S.Q., Yumet, G., Louvi, A., Efstratiadis, A., and Baserga, R. (1997). Insulin-like growth factor II stimulates cell proliferation through the insulin receptor. Proc Natl Acad Sci USA 94, 3777–3782.
Picelli, S., Faridani, O.R., Björklund, A.K., Winberg, G., Sagasser, S., and Sandberg, R. (2014). Full-length RNA-seq from single cells using Smart-seq2. Nat Protoc 9, 171–181.
Rossant, J., and Cross, J.C. (2001). Placental development: lessons from mouse mutants. Nat Rev Genet 2, 538–548.
Schmidt, J.V., Matteson, P.G., Jones, B.K., Guan, X.J., and Tilghman, S.M. (2000). The *Dlk1* and *Gtl2* genes are linked and reciprocally imprinted. Genes Dev 14, 1997–2002.
Sibley, C.P., Coan, P.M., Ferguson-Smith, A.C., Dean, W., Hughes, J., Smith, P., Reik, W., Burton, G.J., Fowden, A.L., and Constância, M. (2004). Placental-specific insulin-like growth factor 2 (Igf2) regulates the diffusional exchange characteristics of the mouse placenta. Proc Natl Acad Sci USA 101, 8204–8208.
Sun, M., Maliqueo, M., Benrick, A., Johansson, J., Shao, R., Hou, L., Jansson, T., Wu, X., and Stener-Victorin, E. (2012). Maternal androgen excess reduces placental and fetal weights, increases placental steroidogenesis, and leads to long-term health effects in their female offspring. Am J Physiol Endocrinol Metab 303, E1373–E1385.
Surani, M.A.H., Barton, S.C., and Norris, M.L. (1984). Development of reconstituted mouse eggs suggests imprinting of the genome during gametogenesis. Nature 308, 548–550.
Takada, S., Paulsen, M., Tevendale, M., Tsai, C.E., Kelsey, G., Cattanach, B.M., and Ferguson-Smith, A.C. (2002). Epigenetic analysis of the Dlk1-Gtl2 imprinted domain on mouse chromosome 12: implications for imprinting control from comparison with Igf2-H19. Hum Mol Genet 11, 77–86.
Takada, S., Tevendale, M., Baker, J., Georgiades, P., Campbell, E., Freeman, T., Johnson, M.H., Paulsen, M., and Ferguson-Smith, A.C. (2000). Delta-like and gtl2 are reciprocally expressed, differentially methylated linked imprinted genes on mouse chromosome 12. Curr Biol 10, 1135–1138.
Tarkowski, A.K. (1975). Induced parthenogenesis in the mouse. Symp Soc Dev Biol, 107–129.
Thorvaldsen, J.L., Duran, K.L., and Bartolomei, M.S. (1998). Deletion of the H19 differentially methylated domain results in loss of imprinted expression of H19 and Igf2. Genes Dev 12, 3693–3702.
Thorvaldsen, J.L., Mann, M.R.W., Nwoko, O., Duran, K.L., and Bartolomei, M.S. (2002). Analysis of sequence upstream of the endogenous H19 gene reveals elements both essential and dispensable for imprinting. Mol Cell Biol 22, 2450–2462.
Tremblay, K.D., Duran, K.L., and Bartolomei, M.S. (1997). A 5′ 2-kilobase-pair region of the imprinted mouse H19 gene exhibits exclusive paternal methylation throughout development. Mol Cell Biol 17, 4322–4329.
Wang, L., and Li, J. (2019). 'Artificial spermatid'-mediated genome editing†. Biol Reprod 336.
Wei, L., Wang, X., Yang, S., Yuan, W., and Li, J. (2017). Efficient generation of the mouse model with a defined point mutation through haploid cell-mediated gene editing. J Genet Genom 44, 461–463.
Wu, Y., Liang, D., Wang, Y., Bai, M., Tang, W., Bao, S., Yan, Z., Li, D., and Li, J. (2013). Correction of a genetic disease in mouse via use of CRISPR-Cas9. Cell Stem Cell 13, 659–662.
Yagi, M., Kishigami, S., Tanaka, A., Semi, K., Mizutani, E., Wakayama, S., Wakayama, T., Yamamoto, T., and Yamada, Y. (2017). Derivation of ground-state female ES cells maintaining gamete-derived DNA methylation. Nature 548, 224–227.
Yan, M., and Li, J. (2019). The evolving CRISPR technology. Protein Cell 550.
Yang, H., Shi, L., Wang, B.A., Liang, D., Zhong, C., Liu, W., Nie, Y., Liu, J., Zhao, J., Gao, X., et al. (2012). Generation of genetically modified mice by oocyte injection of androgenetic haploid embryonic stem cells. Cell 149, 605–617.
Zhang, Y., Xiang, Y., Yin, Q., Du, Z., Peng, X., Wang, Q., Fidalgo, M., Xia, W., Li, Y., Zhao, Z.A., et al. (2018). Dynamic epigenomic landscapes during early lineage specification in mouse embryos. Nat Genet 50, 96–105.
Zhong, C., Xie, Z., Yin, Q., Dong, R., Yang, S., Wu, Y., Yang, L., and Li, J. (2016). Parthenogenetic haploid embryonic stem cells efficiently support mouse generation by oocyte injection. Cell Res 26, 131–134.
Zhong, C., Yin, Q., Xie, Z., Bai, M., Dong, R., Tang, W., Xing, Y.H., Zhang, H., Yang, S., Chen, L.L., et al. (2015). CRISPR-Cas9-mediated genetic screening in mice with haploid embryonic stem cells carrying a guide RNA library. Cell Stem Cell 17, 221–232.

SUPPORTING INFORMATION

Figure S1 Characterizations of WT and DKO AG-haESCs.

Figure S2 RNA-seq analysis of SC blastocysts.

Figure S3 *H19*-DMR and *IG*-DMR deletions (DKO) enhance SC embryonic development.

Figure S4 Abnormal development of SC embryos derived from $IG^{\Delta DMR}$-AG-haESCs.

Figure S5 Characterizations of $H19^{\Delta 13kb}$-AG-haESCs.

Figure S6 Correlation between hypomethylation of *IG*-DMR and growth retardation of SC embryos from $H19^{\Delta 13kb}$-AGH-OG3 cells at late-gestation.

Figure S7 RNA-seq analysis of placentas with different DNA/gene deletions.

Figure S8 Characterizations of TKO AG-haESCs.

Table S1 List of primers and sgRNA sequences in this study

The supporting information is available online at http://life.scichina.com and https://link.springer.com. The supporting materials are published as submitted, without typesetting or editing. The responsibility for scientific accuracy and content remains entirely with the authors.